J|A|C|S ARTICLES

Published on Web 04/16/2010

Rational Synthesis of Heterostructured Nanoparticles with Morphology Control

Chao Wang,*[,†,‡] Wende Tian,[§] Yong Ding,[||] Yu-qiang Ma,[§] Zhong Lin Wang,[||] Nenad M. Markovic,[‡] Vojislav R. Stamenkovic,[‡] Hideo Daimon,[⊥] and Shouheng Sun*[,†]

Department of Chemistry, Brown University, Providence, Rhode Island 02912, Materials Science Division, Argonne National Laboratory, Argonne, Illinois 60439, National Laboratory of Solid State Microstructures, Nanjing University, Nanjing 210093, People's Republic of China, School of Materials Science and Engineering, Georgia Institute of Technology, Atlanta, Georgia 30332-0245, and Fundamental Technology Center, Technology & Development Division, Hitachi Maxell, Ltd., 1-1-88 Ushitora, Ibaraki, Osaka 567-8567, Japan

Received February 12, 2010; E-mail: chaowang@anl.gov; ssun@brown.edu

Abstract: Rational synthesis of Pt−Au$_n$ nanoparticles (NPs) has been achieved by overgrowing Au on Pt with *n*, the number of Pt−Au heterojunctions in each particle, controlled from 1 to 4, and the corresponding NPs in pear-, peanut-, or clover-like morphology. Monte Carlo simulation reveals that the morphology control can be correlated to a thermodynamic equilibrium of the Au coherence energy, the overall particle surface energy, and the heterogeneous Pt−Au interfacial energy in the composite system, which is manipulated by the seeding particle size and solvent polarity. The developed synthetic strategy together with the provided fundamental understanding of heterogeneous nucleation and heterostructure growth could have great potential toward the rational synthesis of composite nanomaterials with morphology control for advanced catalytic and other functional applications.

Introduction

The rational synthesis of nanomaterials in controlled morphology has long been pursued to tailor material properties for advanced electronic,[1−6] magnetic,[7−10] biomedical,[11−15] and energy conversion[16−20] applications. Such a control has been extensively studied in single-component NPs,[21,22] where a primary understanding of the mechanisms governing the shaped growth has been established, though mostly still in an empirical stage. A more challenging target is to achieve the growth of heterostructures with shape control to the same extent as realized in single-component systems.

Dumbbell-like nanoparticles (NPs) represent an important type of heterogeneous nanostructure,[23−27] which contain two

† Brown University.
‡ Argonne National Laboratory.
§ Nanjing University.
|| Georgia Institute of Technology.
⊥ Hitachi Maxell, Ltd.

(1) Choi, C. L.; Koski, K. J.; Sivasankar, S.; Alivisatos, A. P. *Nano Lett.* **2009**, *9*, 3544–3549.
(2) Kan, S.; Mokari, T.; Rothenberg, E.; Banin, U. *Nat. Mater.* **2003**, *2*, 155–158.
(3) Lu, W.; Lieber, C. M. *Nat. Mater.* **2007**, *6*, 841–850.
(4) Peng, X. G.; Manna, L.; Yang, W. D.; Wickham, J.; Scher, E.; Kadavanich, A.; Alivisatos, A. P. *Nature* **2000**, *404*, 59–61.
(5) Wang, C.; Hu, Y. J.; Lieber, C. M.; Sun, S. H. *J. Am. Chem. Soc.* **2008**, *130*, 8902–8903.
(6) Yu, H.; Li, J. B.; Loomis, R. A.; Wang, L. W.; Buhro, W. E. *Nat. Mater.* **2003**, *2*, 517–520.
(7) Puntes, V. F.; Krishnan, K. M.; Alivisatos, A. P. *Science* **2001**, *291*, 2115–2117.
(8) Chen, M.; Kim, J.; Liu, J. P.; Fan, H. Y.; Sun, S. H. *J. Am. Chem. Soc.* **2006**, *128*, 7132–7133.
(9) Lu, A. H.; Salabas, E. L.; Schuth, F. *Angew. Chem., Int. Ed.* **2007**, *46*, 1222–1244.
(10) Wang, C.; Hou, Y. L.; Kim, J. M.; Sun, S. H. *Angew. Chem., Int. Ed.* **2007**, *46*, 6333–6335.
(11) Cheng, K.; Peng, S.; Xu, C. J.; Sun, S. H. *J. Am. Chem. Soc.* **2009**, *131*, 10637–10644.
(12) Chithrani, B. D.; Ghazani, A. A.; Chan, W. C. W. *Nano Lett.* **2006**, *6*, 662–668.
(13) Lim, J. K.; Tan, D. X.; Lanni, F.; Tilton, R. D.; Majetich, S. A. *J. Magn. Magn. Mater.* **2009**, *321*, 1557–1562.
(14) Wang, H. F.; Huff, T. B.; Zweifel, D. A.; He, W.; Low, P. S.; Wei, A.; Cheng, J. X. *Proc. Natl. Acad. Sci. U.S.A.* **2005**, *102*, 15752–15756.
(15) Yavuz, M. S.; Cheng, Y. Y.; Chen, J. Y.; Cobley, C. M.; Zhang, Q.; Rycenga, M.; Xie, J. W.; Kim, C.; Song, K. H.; Schwartz, A. G.; Wang, L. H. V.; Xia, Y. N. *Nat. Mater.* **2009**, *8*, 935–939.
(16) Tian, N.; Zhou, Z. Y.; Sun, S. G.; Ding, Y.; Wang, Z. L. *Science* **2007**, *316*, 732–735.
(17) Wang, C.; Daimon, H.; Lee, Y.; Kim, J.; Sun, S. *J. Am. Chem. Soc.* **2007**, *129*, 6974–6975.
(18) Chen, J. Y.; Lim, B.; Lee, E. P.; Xia, Y. N. *Nano Today* **2009**, *4*, 81–95.
(19) Peng, Z. M.; Yang, H. *Nano Today* **2009**, *4*, 143–164.
(20) Tsung, C. K.; Kuhn, J. N.; Huang, W. Y.; Aliaga, C.; Hung, L. I.; Somorjai, G. A.; Yang, P. D. *J. Am. Chem. Soc.* **2009**, *131*, 5816–5822.
(21) Burda, C.; Chen, X. B.; Narayanan, R.; El-Sayed, M. A. *Chem. Rev.* **2005**, *105*, 1025–1102.
(22) Jun, Y. W.; Choi, J. S.; Cheon, J. *Angew. Chem., Int. Ed.* **2006**, *45*, 3414–3439.
(23) Gu, H. W.; Zheng, R. K.; Zhang, X. X.; Xu, B. *J. Am. Chem. Soc.* **2004**, *126*, 5664–5665.
(24) Kwon, K. W.; Shim, M. *J. Am. Chem. Soc.* **2005**, *127*, 10269–10275.
(25) Yu, H.; Chen, M.; Rice, P. M.; Wang, S. X.; White, R. L.; Sun, S. H. *Nano Lett.* **2005**, *5*, 379–382.
(26) Shi, W. L.; Zeng, H.; Sahoo, Y.; Ohulchanskyy, T. Y.; Ding, Y.; Wang, Z. L.; Swihart, M.; Prasad, P. N. *Nano Lett.* **2006**, *6*, 875–881.

 10.1021/ja101305x

different particles that are epitaxially linked and have two different types of material surface. Such heterostructured NPs are commonly obtained by sequential growth of a second NP on the preformed seeding particles, where the nucleation and growth are anisotropically centered on one specific crystal plane around the seeding NPs, not uniformly distributed as in the case of core/shell structures. Therefore, the synthesis of dumbbell-like NPs relies critically on promoting the heterogeneous nucleation while suppressing the homogeneous nucleation. This can be achieved by tuning the seed-to-precursor ratio and controlling the heating profile so that the concentration of the precursors is below the homogeneous nucleation threshold throughout the synthesis.[28] The lattice spacings of the two NPs are generally matched at interface(s) to lower the energy required for overgrowth of the second component.[24] The crystal and electronic structures of one NP can be locally modified by the other NP through the interactions at the interface, providing an additional degree of freedom for tailoring material properties.[27] Fruthermore, the presence of more than one type of materials in a single nanostructure makes them ideal candidates for multifunction applications.[29] Despite the progress in synthesis of heterostructured NPs of various types of materials,[27] rational control of the composite particle morphology, e.g. the number of heterojunctions within each NP, is still difficult to realize.

Here we report the synthesis of heterostructured Pt−Au$_n$ NPs by overgrowing Au on Pt NPs with n (=1 ∼ 4) representing the number of Pt−Au heterojunctions in each particle. The size of the seeding NPs and the polarity of the solvent have been systematically tuned to investigate their effects on the heterogeneous nucleation and control the morphology of Pt−Au$_n$ NPs. A fundamental understanding of the rational control of heterojunction formation is provided by a Monte Carlo simulation. The junction effect within the heterostructure is further studied by applying the Pt−Au$_n$ NPs as electrocatalysts for the methanol oxidation reaction.

Experimental Section

Synthesis. Pt NPs (3, 5, and 7 nm) were synthesized according to the procedures described in a previous publication.[30] For the synthesis of Pt−Au$_4$ NPs, 0.1 g of $HAuCl_4$ was dissolved in 20 mL of 1-octadecene in the presence of 2 mL of oleylamine by magnetic stirring. Under the protection of nitrogen, 20 mg of 7 nm Pt NPs dispersed in hexane were added into the solution at 60 °C. Au overgrowth was carried out at this temperature for 5 h. After the mixture was cooled to room temperature, 40 mL of isopropyl alcohol was added to the reaction mixture to precipitate the NPs and the product was collected by centrifuge (6000 rpm, 6 min). The size of the Au particle is 10 nm (for each Au branch) in the obtained Pt−Au$_4$ NPs. Pt−Au$_2$ and Pt−Au$_1$ NPs were obtained by the same recipe, but with 5 and 3 nm Pt NPs as seeds, respectively. A statistical summary of the number of Au branches in each particle for the various shape-controlled NPs is shown in Figure S1 (Supporting Information).

Characterization. TEM images were acquired on a Philips EM 420 transmission electron microscope (TEM, with an accelerating voltage of 120 kV). High-resolution TEM (HRTEM) images were recorded by a JEOL JEM-2010 and a JEOL JEM4000EX microscope (with accelerating voltages of 200 and 400 kV, respectively). X-ray diffraction (XRD) patterns of the particle assemblies were collected on a Bruker AXS D8 Advance Diffractometer with Cu Kα radiation (λ = 1.5418 Å).

Electrocatalytic study was performed at room temperature on a Fuel Cell Electrocatalyst RRDE Bundle from Pine Instrument Co. The as-synthesized Pt−Au NPs were washed three times with ethanol, and ∼20 mg of NPs was dispersed in 10 mL of 0.1% tetramethylammonium hydroxide solution with sonication. When 20 μL of acetic acid was added, the NPs were precipitated out by centrifuge. This process was repeated three times to remove the organic surfactants.[31] The NPs were mixed with 40 mg of carbon black (Ketjen Black EC, Lion) in 50 mL of deionized water by sonication, and 50 μL of the suspension was dropped onto a glassy-carbon disk (6 mm in diameter). A typical three-electrode cell was set up with a glassy-carbon disk as the working electrode, Pt wire as the counter electrode, and Ag/AgCl as the reference electrode. Cyclic voltammetry (CV) was first carried out in Ar-purged 0.5 M H_2SO_4 with a scanning rate of 50 mV/s and used to evaluate the active surface area of the Pt catalyst. Methanol oxidation reaction activity was measured in Ar-purged 0.5 M aqueous H_2SO_4 containing 1 M CH_3OH with a scanning rate of 50 mV/s.

Monte Carlo Simulation. The modeling followed the approach described by Mokari et al.[32] The system was represented by a two-dimensional (size 300 × 300) lattice. Each cell of the square lattice can be occupied by Pt, Au, or the solvent. The density of gold and solvent is represented by the two binary variables g_i = 0, 1 and l_i = 0, 1, respectively, with 1 indicating occupation while 0 no occupation at site i. The Pt seed is modeled by s_i = 0, 1 in the same way.

Nonequilibrium initial conditions were adopted to simulate the experiments. The initial distribution of Au is uniform and random, described as

$$g_i = \begin{cases} 1, \xi < \rho_g \\ 0, \text{otherwise} \end{cases}$$

where ξ is in the range [0: 1] and $0 \le \rho_g \le 1$ is the gold density. A single square with dimensions $L \times L$ (here L is the edge length in lattice unit) is used to represent the Pt seed, with $s_i = 1$ in the square and $s_i = 0$ otherwise. The corners of the square were modified as half-circled caps to prevent the growth of rectangular-shaped gold tips in the early stage resulting from the choice of the symmetry of our lattice. Gold species interact with the solvent, the square seed, and each other, following a Metropolis probability P_{acc} = min[1,exp(−$\Delta H/k_BT$)], where k_B is Boltzmann's constant and ΔH is the resulting change in energy. The Hamiltonian of the system is described by

$$\begin{aligned} H &= H_l + H_g + H_{gl} + H_{gs} \\ &= -\epsilon_l \sum_{\langle ij \rangle} l_i l_j - \epsilon_g \sum_{\langle ij \rangle} \gamma_{ij} g_i g_j - \epsilon_{gl} \sum_{\langle ij \rangle} g_i l_j - \epsilon_{gs} \sum_{\langle ij \in \text{cap} \rangle} g_i s_j \end{aligned} \quad (1)$$

with sums including only nearest-neighbor cells. The liquid−liquid attraction was set as $\epsilon_l = (2/3)T$, gold−gold attraction $\epsilon_g = (2/3)T$, gold−liquid attraction $\epsilon_{gl} = (4/3)T$, and gold−seed attraction $\epsilon_{gs} = 25T$, where T is the temperature. Gold−seed attraction is spatially limited to only the tips to mimic the preferential growth along ⟨111⟩ directions. The parameter $\gamma_{ij} = (\gamma_i\gamma_j)^{1/2}$ represents the dependence of the gold−gold interaction strength on the oxidation state of the gold: $\gamma_i = 6$ for Au^0 or $\gamma_i = 1$ otherwise. Qualitatively the results are insensitive to these parameters within a reasonable range as

(27) Wang, C.; Xu, C. J.; Zeng, H.; Sun, S. H. *Adv. Mater.* **2009**, *21*, 3045–3052.
(28) Murray, C. B.; Kagan, C. R.; Bawendi, M. G. *Annu. Rev. Mater. Sci.* **2000**, *30*, 545–610.
(29) Xu, C. J.; Wang, B. D.; Sun, S. H. *J. Am. Chem. Soc.* **2009**, *131*, 4216–4217.
(30) Wang, C.; Daimon, H.; Onodera, T.; Koda, T.; Sun, S. H. *Angew. Chem., Int. Ed.* **2008**, *47*, 3588–3591.
(31) Liu, Z.; Reed, D.; Kwon, G.; Shamsuzzoha, M.; Nikles, D. E. *J. Phys. Chem. C* **2007**, *111*, 14223–14229.
(32) Mokari, T.; Sztrum, C. G.; Salant, A.; Rabani, E.; Banin, U. *Nat. Mater.* **2005**, *4*, 855–863.

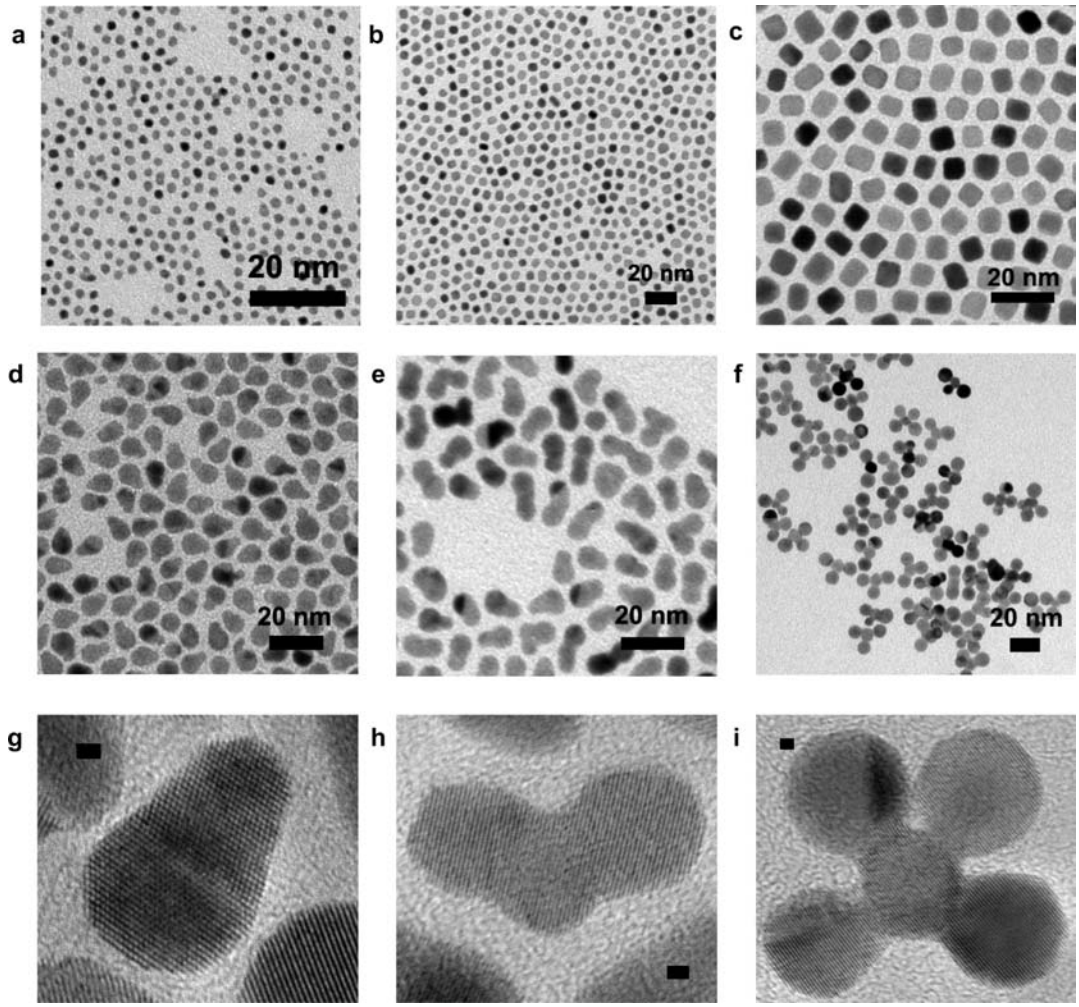

Figure 1. Image analysis of Pt−Au_n NPs: (a−c) TEM images of 3 nm (a), 5 nm (b) and 7 nm (c) Pt seeds; (d−i) TEM and HRTEM images of 3−8 nm pearlike (d, g), 5−8 nm peanutlike (e, h), and 7−10 nm cloverlike (f, i) Pt−Au NPs. Scale bars in (g)−(i) are equal to 1 nm.

long as (i) the gold−gold sticking probability in solution is small ($\epsilon_l < \epsilon_{gl}$) and (ii) the gold−seed sticking probability is large ($\epsilon_{gs} > \epsilon_{gl}$).

All images were obtained after 60 000 000 Monte Carlo steps, at which point the particle morphology becomes stable. A movie of the particle morphology evolution is provided in the Supporting Information.

Results and Discussion

Heterostructured Pt−Au_n NPs were synthesized through a seed-mediated process. In the presence of Pt NPs as seeds, $HAuCl_4$ was reduced by oleylamine in 1-octadecene and epitaxially grown on Pt. The size of Pt seeds was tuned from 3 to 7 nm (Figure 1a−c) to investigate its effect on the morphology of Pt−Au NPs. The epitaxial growth of Au on 3 nm Pt seeds gave pearlike 3−8 nm Pt−Au_1 NPs, as shown by the TEM image in Figure 1d. Use of 5 nm Pt NPs as seeds led to peanutlike 5−8 nm (the size of Au NPs is referred to each single Au particle in the heterostructure) Pt−Au_2 NPs (Figure 1e), and 7 nm Pt induced the formation of cloverlike 7−10 nm Pt−Au_n ($n = 3$, 4, Figure 1f). Corresponding HRTEM images (Figure 1g−i) show coherent lattice fringes across the NPs with negligible contrast between the Pt seeds and the grown Au branches, because of the close atomic numbers (78 for Pt and 79 for Au) and lattice constants (both are face-centered cubic (fcc): 3.92 Å for Pt and 4.08 Å for Au). The interfringe distances were measured to be 0.22−0.23 nm in all three types of NPs, which are related to (111) planes of either Pt or Au in the fcc phase. It is worth pointing out that the lattice coherence between Pt and Au observed here is different from the previous report by growing Au over Pt cubes in aqueous solution at room temperature where a great number of crystal defects were observed at the interface and Au nanorods were obtained.[33] It seems that the rather high temperature (60 °C) in our synthesis, in addition to the different solvent used (organic hydrocarbon liquid vs water), helps eliminate defect formation, giving well-crystallized interfaces.

Pt and Au in the nanostructure was distinguished by inverse Fourier transform applied to the HRTEM images of the NPs. Figure 2a shows the HRTEM image of a typical cloverlike Pt−Au_4 NP. The whole particle shows coherent lattice fringes, except the lower right branch, which is in a misaligned crystal orientation. Figure 2b shows the diffractogram pattern calculated from the particle shown in Figure 2a. From a close view of the diffraction spots, e.g. (111) as shown in the inset, we can see that it actually has two separated smaller spots due to the slightly different (111) planar distances of the Pt and Au crystals. Selectively applying inverse Fourier transform to these two spots gives the real-spatial distribution of Pt (Figure 2c) and Au

(33) Habas, S. E.; Lee, H.; Radmilovic, V.; Somorjai, G. A.; Yang, P. *Nat. Mater.* **2007**, *6*, 692–697.

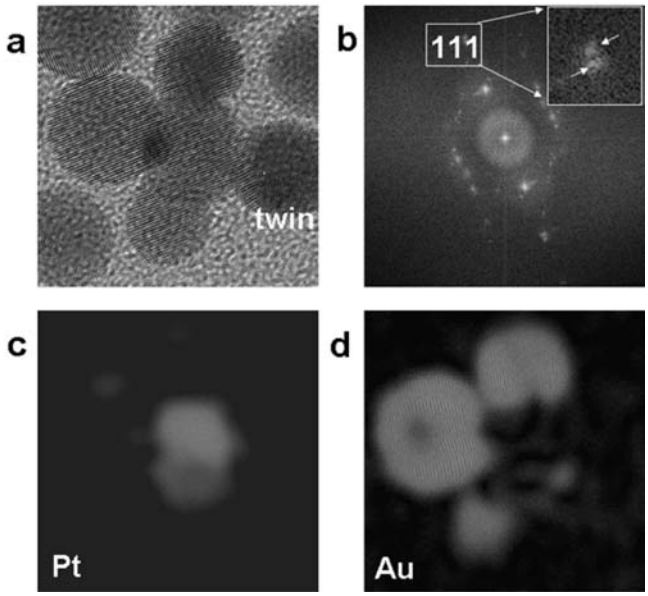

Figure 2. Fourier-transform and inverse-Fourier-transform analyses for HRTEM images of Pt−Au NPs: HRTEM image (a) and diffractogram pattern (b) of a single 7−10 nm cloverlike Pt−Au_4 NP. The inset in (b) shows the split of the (111) peak into two spots, comprising one for Pt and the other one for Au particles. Each of them can provide the information of spatial distribution for Pt (or Au) after an inverse Fourier transform. (c) and (d) are the images of Pt and Au particles obtained by such an approach.

(Figure 2d), respectively. It becomes obvious that, in the cloverlike structure, four Au particles grow on one Pt particle. The Au particle at the lower right corner in Figure 2d is "missed" because of its misaligned crystal orientation compared with others. A similar observation has been made when the technique was applied to the other Pt−Au NPs.

The nanostructure has been further characterized by X-ray diffraction (XRD). Figure S2 (Supporting Information) shows the XRD patterns of the three kinds of Pt−Au composite NPs. Two sets of peaks are present, which can be ascribed to fcc Pt and Au by comparison with the standard peaks. The (111) peaks for Pt and Au are very close to each other, again due to the small lattice mismatch between Au and Pt (<5%). For the 3−8 nm Pt−Au NPs, the peaks for Pt are almost buried in Au peaks due to the much smaller size of Pt as compared to that of Au. The Pt (111) and (200) peaks become more visible in 5−8 and 7−10 nm Pt−Au NPs, as the size of Pt in the composite NPs increases.

To understand the growth mechanism, we first performed control experiments to investigate the effect of precursor ratio on the Pt−Au particle morphology. One might predict that alteration of the ratio between the Au salt and Pt seeds could modulate the heterogeneous nucleation and thus control the number of Au branches grown on each Pt particle. However, this is not the case. In the growth of the cloverlike Pt−Au NPs shown in Figure 1f, 0.1 g of $HAuCl_4$ was used while the added seeds were 20 mg of 7 nm Pt NPs (see the Experimental Section). Pt−Au nanostructures with three to four Au branches on each Pt were still obtained when the amount of $HAuCl_4$ was reduced to 0.02 g and the amount of Pt seeds was kept the same (Figure S3a, Supporting Information). It was also similar by keeping the Au precursor constant while the amount of Pt seeds was reduced to 5 mg, except that some free Au NPs were formed (Figure S3b). Tuning the precursor ratio did not change the morphologies (the same number of Au branches) for the other

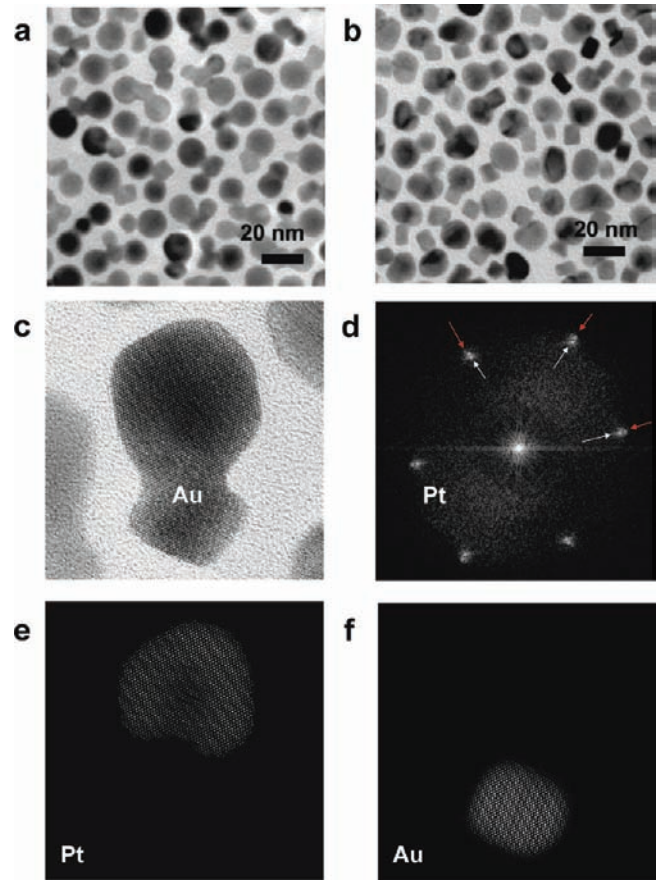

Figure 3. (a, b) TEM images of Pt−Au NPs from growth in diphenyl ether (a) and chloroform (b). (c−f) Fourier-transform analyses of a 7−10 nm dumbbell-like Pt−Au NP: HRTEM image (c), diffractogram pattern (d) of the NP, and spatial distribution of Au (e) and Pt (f).

shapes of Pt−Au NPs either. Therefore, the morphology control of Pt−Au_n NPs is unlikely directed by the ratio between precursors.

From the structure characterization of the NPs (Figures 1 and 2), we can see that the epitaxial growth of Au on Pt seeds preferentially happens on Pt (111) planes. This seems to be consistent with the previous observations in the synthesis of Pt nanocubes in the presence of oleylamine, where growth along the ⟨111⟩ directions is faster than that along ⟨100⟩ and the other directions, due to the selective binding of the surfactant on different crystal facets.[17,34] In the case of the Pt−Au system, the material difference between the seed and overgrown particle might not hinder this favored ⟨111⟩ growth because of the rather small lattice mismatch between Pt and Au (111) planes (Table S1, Supporting Information). This effect can explain the spatial distribution of Au branches around Pt seeds in tetrahedron-like and "V-shaped" arrangements, instead of forming core/shell NPs.

Solvent polarity is another important factor in controlling heterogeneous nucleation.[25] Figure 3 shows the TEM images of Pt−Au NPs obtained when the synthesis was performed in a more polar solvent, such as diphenyl ether (Figure 3a) or chloroform (Figure 3b), with all the other reaction conditions kept the same as those for Pt−Au_4 cloverlike NPs (Figure 1f). HRTEM images and SAED analysis of the nanostructures (Figure 3c−f) reveal that the growth was also epitaxial along

(34) Ren, J. T.; Tilley, R. D. *J. Am. Chem. Soc.* **2007**, *129*, 3287–3291.

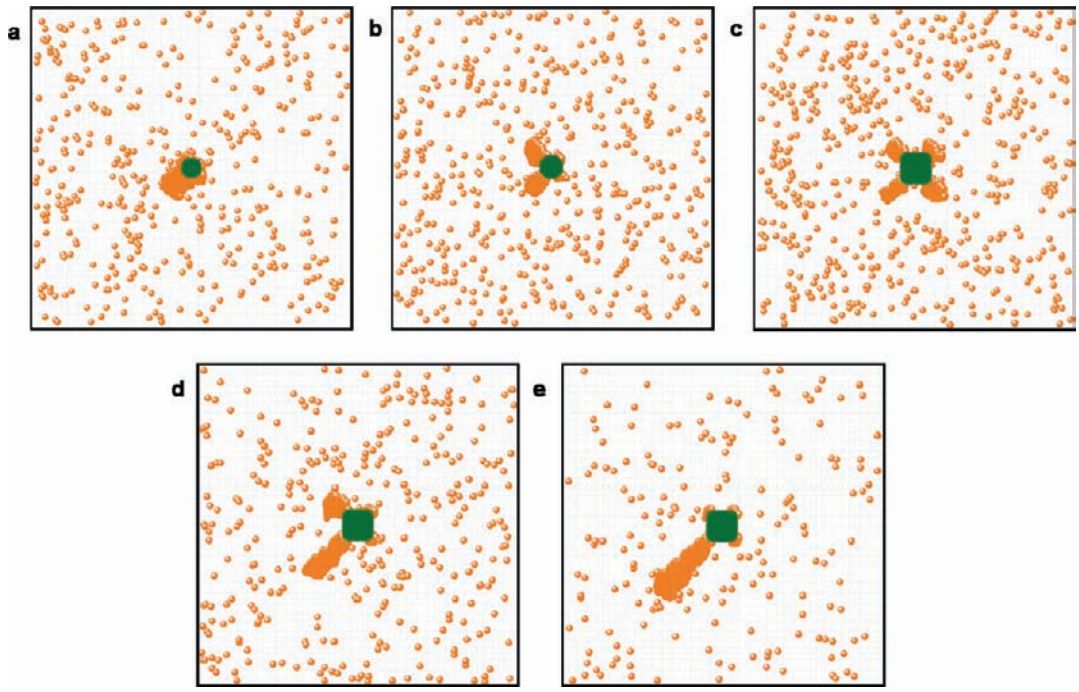

Figure 4. Theoretical modeling showing the Pt−Au NPs morphologies from growth with 3 nm (a), 5 nm (b), and 7 nm (c) Pt seeds in octadecene and in 7 nm Pt seeds in diphenyl ether (d) and chloroform (e).

the ⟨111⟩ directions. However, the number of Au particles associated with each Pt NP is increased as a more nonpolar solvent was used. Pt−Au NPs with only one Au branch in each NP were obtained from the synthesis in chloroform (dipole moment 1.5 D), while mostly two branches were obtained in diphenyl ether (diple moment 1.05 D), compared with three- or four-branch structures in 1-octadecene (diple moment: 0.47 D).

A better understanding of the morphology-controlled growth mechanism was provided by a theoretical simulation of the NP growth in a lattice−gas model (see the Experimental Section). By representing the system in a two-dimensional lattice, this model has been proved to be simple but successful in depicting the thermodynamic and kinetic process of nanocrystal growth in the solution phase.[32] Figure 4a−c shows the thermal equilibrium morphologies of Pt−Au NPs obtained in 1-octadecene. In a 300 × 300 lattice, 3, 5, and 7 nm Pt seeding NPs were represented by a disk with radius of 14 (Figure 4a), a 22 × 22 hexagon (Figure 4b), and a 30 × 30 square (Figure 4c), respectively, to mimic the size and morphology of seeding NPs.[35] Strikingly, the simulation results are in agreement with the experimental observations (Figure 1) that as the size of Pt seeds increased, the shape of Pt−Au NPs evolves from pear to peanut and clover.

(35) The 3 and 5 nm Pt seeds can be viewed as spherical and truncated cubic shapes, respectively. The overgrowth of Au was assumed to be preferentially over Pt {111} planes by restricting the growth along diagonal directions (related to the orthogonal lattice) of the cube and hexagon. However, such a restriction is unnecessary for a sphere, since it has no anisotropy for overgrowth. The assumption is based on the rather small lattice mismatch along the ⟨111⟩ direction between fcc Au and Pt, which is also supported by the fact that epitaxial growth along ⟨111⟩ is much faster than that along other directions for fcc Pt[34] and the previous observation. (Wang, C. *J. Am. Chem. Soc.* **2008**, *129*, 6974) that oleylamine/oleic acid may bind more strongly on Pt (100) than on Pt (111). Similar treatment was also used in the previous studies.[2]

In a close view of the theoretical model we found that the seed-dependent growth of Pt−Au NPs into different morphologies was regulated by a thermodynamic equilibrium between the particle surface energy and the Pt−Au heterogeneous interfacial energy, which correspond to H_{gl} and H_{gs} in the model, respectively (eq 1, see the Experimental Section). In the above we have depicted that Au tends to epitaxially grow over Pt along the ⟨111⟩ directions. This provides the intrinsic driving force for multiple and separate nucleation of Au over Pt. However, the NP growth in the real case has to be further regulated by thermodynamics. As the seeding particle size increases, the overall energy of the Pt−Au structure becomes dominated by the interfacial energy, as reflected by the expanded sum for H_{gs} in eq 1 due to interface area enlargement. As a consequence, the weight of the surface energy (mostly contributed by the Au particle surface, H_{gl}) becomes minor and thus allows the growth of Au into separate particles on multiple facets (with larger surface area than a single, big Au particle).

Another way to manipulate the growth thermodynamics is to tune the solvent polarity, which is reflected by the Au−liquid attraction ϵ_{gl} in the system. The surfactants, oleylamine and oleic acid, on the NPs surface have long hydrophobic/neutral hydrocarbon chains stretching outside, and thus the interaction between them and the solvent (ϵ_{gl}) should be reduced as the polarity of the solvent increases. Figure 4c−e shows the Pt−Au$_n$ nanostructures with $n = 4$ (Figure 4c), 2 (Figure 4d), and 1 (Figure 4e) by setting ϵ_{gl} as 0.95, 0.85, and 0.70 to simulate the solvents of 1-octadecene, diphenyl ether, and chloroform, respectively, while all the other conditions are kept the same as those for Figure 4c. The observations are consistent with the experimental results stated above (Figure 3). In this case the two terms in competition in eq 1 are H_g and H_{gl} (H_{gs} can be regarded as fixed for the same seed). As ϵ_{gl} decreases, the Au coherence energy H_g becomes comparable or even weights over

the surface energy H_{gl}, which drives the overgrowth of Au into a single and large particle, instead of several small ones.

The obtained composite NPs with a controlled number of heterojunctions enable the study of the heterogeneous interfacial interactions at the nanoscale. We have demonstrated that the morphology of the Pt−Au$_n$ NPs has a direct effect on their catalytic properties. Figure S4 (Supporting Information) shows the catalytic activities of pearlike Pt−Au$_1$ (Figure 3b) and cloverlike Pt−Au$_4$ (Figure 1f) NPs for the methanol oxidation reaction, in comparison with the 7 nm Pt seeding NPs. The current densities were obtained by normalizing the measured current with the electrochemical surface area calculated from their CVs.[30] Both cloverlike Pt−Au$_4$ and pearlike Pt−Au$_1$ NPs show higher peak current density than Pt particles, indicating the platinum atom on the heterostructured NPs has higher methanol oxidation reaction activity than its counterpart on single-component Pt NPs, while those on Pt−Au$_4$ are even more active than for Pt−Au$_1$ NPs, as indicated by a difference of ~0.6 mA/cm^2 at a potential of 0.8 V (Figure S4a). After holding the potential at 0.8 V for 2 h, the current density of cloverlike NPs was still as high as 0.8 mA/cm^2 (~50% of the initial value) while that of pearlike Pt−Au$_1$ dropped to below 0.5 mA/cm^2 (~40% of the initial value), in comparison with <0.25 mA/cm^2 (less than 25% of the initial value) for the Pt catalyst (Figure S4b). Though the detailed mechanism is yet unclear, the observed activity enhancement could originate from the partial electron deficiency of Pt in the Pt−Au NPs due to the electron transfer from the Pt to Au between their Fermi levels across the interface (Figure S5, Supporting Information). Such an electron transfer could be more prominent in Pt−Au NPs with more Au branches.[25]

Conclusions

We have developed a novel route toward heterostructured Pt−Au$_n$ nanoparticles with the number of Pt−Au heterojunctions in each particle (n) controlled from 1 to 4 and the corresponding particle in cloverlike ($n = 4$), peanutlike ($n = 2$), and pearlike ($n = 1$) shapes by tuning the size of Pt seeds or the solvent polarity. Monte Carlo simulation reveals that the shaped growth is regulated by a thermodynamic equilibrium of the Au coherence energy, the overall particle surface energy, and the heterogeneous Pt−Au interfacial energy in the system. In addition, the morphology of heterostructured NPs has been demonstrated to have a direct effect on their catalytic performance, with cloverlike NPs showing higher methanol oxidation reaction activity than pearlike Pt−Au NPs. These heterostrucutred NPs thus offer an ideal model system for studying nanoscale interfacial interactions and heterogeneous nanocatalysts. The combinational studies of synthetic routes and theoretical modeling have shown that the morphology of heterostructured nanomaterials can be tailored by manipulation of the heterogeneous growth thermodynamics with carefully designed reaction conditions and thus represent a persuasive approach toward the rational synthesis of composite nanomaterials for advanced catalytic and other nanotechnological applications.

Acknowledgment. This project was supported by the NSF/DMR (Grant No. 0606264), the Brown University Seed Fund, and the DOE (No. DE-AC02-06CH11357). The simulation work at Nanjing University was supported by the National Basic Research Program of China (No. 2007CB925101) and the National Natural Science Foundation of China (No. 10974080).

Supporting Information Available: A table and figures detailing more material characterizations and a movie detailing particle evolution. This material is available free of charge via the Internet at http://pubs.acs.org.

JA101305X